Light Water Reactor Sustainability Program

Update of modeling effort directed at mitigation approaches to reactor pressure vessel embrittlement

January 31, 2019

U.S. Department of Energy

Office of Nuclear Energy

Light Water Reactor Sustainability Program

Update of modeling effort directed at mitigation approaches to reactor pressure vessel embrittlement January 31, 2019 Milestone

Senlin Cui (University of Wisconsin–Madison)
Mahmood Mamivand (University of Wisconsin–Madison)

Key Collaborators
G. Robert Odette (University of California, Santa Barbara)

January 31, 2019

Prepared for the
U.S. Department of Energy
Office of Nuclear Energy

SUMMARY

This report has been assembled to address the following milestone due January 31, 2019:

Milestone Number: M4LW-19OR0402054

Title: “Update of modeling effort directed at mitigation approaches to reactor pressure vessel embrittlement”

ACKNOWLEDGEMENTS

This research was sponsored by the United States Department of Energy, Office of Nuclear Energy, for the Light Water Reactor Sustainability Research and Development effort.

CONTENTS

FIGURES

TABLES

ACRONYMS AND NOMENCLATURE

APT	Atom probe tomography
BCC	Body-centered cubic
CD	Cluster dynamics
CM6	Name of different alloy composition used by University of California, Santa Barbara, collaborators
CRP	Cu-rich precipitate
CV	Cross Validation
GKRR	Gaussian Kernel Ridge Regression
LC, LD, LH, LI, LG	Name of different alloy composition used by University of California, Santa Barbara, collaborators
LO	Leave-out
LWR	Light water reactor
KMC	Kinetic Monte Carlo
MNSP	Mn-Ni-Si rich precipitate
PIA	Post-irradiation annealing
RIS	Radiation-induced segregation
RMSD	Root mean square difference
RMSE	Root mean square error
RPV	Reactor pressure vessel
SS	Stainless steel
UMD	Unstable matrix defects

1. INTRODUCTION

The focus of the overall work has been to understand and mitigate embrittlement of RPVs steels. Made primarily by ferritic low-alloy steels, RPVs are permanent components in light water reactors (LWRs) and their irradiation embrittlement is one of the potential barriers to extending the lifetime of light water reactors. Therefore, predicting and having insight into the RPVs embrittlement in extended life conditions play a critical role in LWRs further licensing. In this report, we have made further progress on ongoing projects that use cluster dynamics models to study the RPVs embrittlement and gain insight into extended life conditions. The focus of this report is on Cu precipitation in ferritic alloys. Specifically, to develop models for embrittlement we must improve our models of Cu precipitation to avoid large Cu diffusivity, since Cu precipitates lead to direct embrittlement and help nucleation and therefore control the growth of Mn-Ni-Si embrittling precipitates. This report describes work extending traditional mesoscale approaches for Cu precipitates to include the expected mobility of Cu clusters.

2. EXECUTIVE SUMMARY OF MAJOR RESULTS

1. Adapted cluster dynamics code to include cluster mobility.
2. Applied new code to model Cu precipitation in Fe and obtained an initial model to reproduce selected experimental data.

3. METHODS

3.1 Basic Cluster Dynamics model

Part of the cluster dynamics simulation model has been discussed in previous milestone [1]. The basic methods are included in this report for completeness.

As described in previous milestones, the CD method [2, 3] gives the size distribution of clusters by solving a series of ordinary differential equations as follows:

$$\frac{\partial f(n,t)}{\partial t} = \omega_{n-1,n}^{(+)} f(n-1,t) - \omega_{n,n-1}^{(-)} f(n,t) + \omega_{n+1,n}^{(-)} f(n+1,t) - \omega_{n,n+1}^{(+)} f(n,t), \quad (1)$$

where

$f(n,t)$ = concentration of clusters containing n atoms at time t.

The coefficient $w_{n,n+1}^{(+)}$ s are the rates at which clusters of size n absorb single atoms to grow to size n+1, $w_{n,n-1}^{(-)}$ s are the rates at which clusters of size n emit single atoms to shrink to size n-1, and $\Delta G(n)$ is the formation energy of clusters with n atoms. More details regarding this method can be found in Ref. [2, 3].

For a system containing k precipitating components, the rates of absorption are given by:

$$\omega_{n,n+1}^{(+)} = \left[\sum_{i=1}^{j} \left(\frac{\nu_{i\alpha}^2}{\omega_{n_i;n_i+1}^{(+)}}\right)\right]^{-1}, \quad (2)$$

where

$w_{n_i,n_i+1}^{(+)}$ = rate at which clusters of size n gain one atom of species i.

The parameter $v_{i\alpha}$ accounts for the change in the composition of component i as the cluster grows from size n to $n+1$. It is defined by the following expression:

$$\nu_{i\alpha} = x_{i\alpha} + n\frac{dx_{i\alpha}}{dn}, \quad (3)$$

where

$x_{i\alpha}$ = atomic fraction of component i in clusters of size n.

Here it is assumed that $x_{i\alpha}$ does not change with n, thus $v_{i\alpha}$ equals $x_{i\alpha}$.

For diffusion-limited growth of the clusters, the absorption rate becomes:

$$\omega_{n,n+1}^{(+)} = 4\pi c_\beta a_\alpha D_{eff}^d n^{1/3}, \quad (4)$$

$$\frac{1}{D_{eff}^{d}} = \sum_{i=1}^{k} \frac{\nu_{i\alpha}^{2}}{x_{i\beta} D_i}, \tag{5}$$

where

C_β = total volume concentration of the particles of the different components in the ambient phase

$x_{i\beta}$ = molar fraction of the different components in the ambient phase.

The emission rate is given by:

$$\omega_{n+1,n}^{(-)} = \omega_{n,n+1}^{(+)} \exp\left(\frac{\Delta G(n+1) - \Delta G(n)}{k_B T}\right), \tag{6}$$

where

$\Delta G(n)$ = formation energy of clusters with n atoms from the matrix, which can be written as:

$$\Delta G(n) = n(g_p - \sum_i x_i \mu_i) + \sigma(n), \tag{7}$$

where

g_p = free energy per atom of the precipitate phase

μ_i = chemical potential of component i in the matrix

$\sigma(n)$ = interfacial energy of a cluster of size n.

With this form, the difference $\Delta G(n+1)$-$\Delta G(n)$ reduces to:

$$\Delta G(n+1) - \Delta G(n) = g_p - \sum_i x_i \mu_i + [\sigma(n+1) - \sigma(n)], \tag{8}$$

The chemical potentials can be written as:

$$\mu_i = \mu_i^0 + kT[ln\gamma_i + lnc_i], \tag{9}$$

Where γ_i is the activity coefficient. When the matrix phase is in equilibrium with the precipitate phase we have the relationship:

$$\begin{aligned} &g_p - \textstyle\sum_i x_{i\alpha} \mu_i = 0 \\ &g_p - \sum_i x_{i\alpha}[\mu_i^0 + kTln\gamma_i] = kT \sum_i x_{i\alpha} ln\bar{c_i} \end{aligned} \tag{10}$$

In dilute alloys, the γ_i in Eq. (9) will become constant according to Henry's law, thus according to Eq. (8) - (10), we can obtain

$$\Delta G(n+1) - \Delta G(n) = kT \textstyle\sum_i x_{i\alpha} ln \frac{\bar{c_i}}{c_i} + [\sigma(n+1) - \sigma(n)], \tag{11}$$

Substituting Eq. (11) into Eq. (6), the emission rate can be written as:

$$\omega_{n+1,n}^{(-)} = \omega_{n,n+1}^{(+)} \frac{\overline{\prod_i c_i^{x_i}}}{\prod_i c_i^{x_i}} \exp\left(\frac{\sigma(n+1)-\sigma(n)}{k_B T}\right), \tag{12}$$

where $\prod_i c_i^{x_i}$ and $\overline{\prod_i c_i^{x_i}}$ are the solute product and solute product at equilibrium, respectively, and they are represented by K_{sp} and $\overline{K_{sp}}$, respectively.

The distribution function f(n=1, t) at n=1 is described as:

$$f(n=1,t) = c_\beta \prod_{i=1}^{k} x_{i\beta}^{x_{i\alpha}}, \tag{13}$$

3.2 Extension of Cluster Dynamics model to mobile clusters

Here we extend the cluster dynamic theory in the framework of Slezov [2, 3] to include cluster diffusivity up to cluster size n_{max}, as well as the limiting case where all the clusters are mobile. If the clusters with size up to n_{max} are mobile, the continuity equation is then given in the form [4]:

$$\frac{\partial f(n,t)}{\partial t} = \sum_{m=1}^{min\,(n-1,n_{max})} J_{(n-m)+(m),(n)} - \sum_{m=1}^{n_{max},n+m\le n_{total}} J_{(n)+(m),(n+m)} - \sum_{m=1}^{n_{total}-n} J_{(m)+(n),(m+n)} \tag{14}$$

If all the clusters are diffusive, then the continuity equation is given as:

$$\frac{\partial f(n,t)}{\partial t} = \sum_{m=1}^{n-1} J_{(n-m)+(m),(n)} - \sum_{m=1}^{n_{total}-n} J_{(n)+(m),(n+m)} - \sum_{m=1}^{n_{total}-n} J_{(m)+(n),(m+n)} \tag{15}$$

where $J_{(n)+(m),(n+m)}$ follows the similar definition of $J_{(n)+(1),(n+1)}$ as:

$$J_{(n)+(m),(n+m)} = w_{(n)+(m),(n+m)}^{(+)} f(n,t) - w_{(n+m)-(m),(n)}^{(-)} f(n+m,t) \tag{16}$$

In Eq. (16), clusters with size m are considered as diffusing and n_{total} is the total number of cluster classes considered during the simulation. The absorption coefficients $w_{(n)+(m),(n+m)}^{(+)}$ are defined following that of single particles as:

$$w_{(n)+(m),(n+m)}^{(+)} = 4\pi R^2 \frac{D_m^*}{\alpha_{m\beta}} c_{m\beta} \left\{ \frac{1}{1+\left[\left(\frac{D_m^*}{D_{(m)}}\right)\left(\frac{R}{\alpha_{m\beta}}\right)\right]} \right\} \tag{17}$$

where R is the capture radius, D_m^* is the partial diffusivity of clusters with size m, $\alpha_{m\beta}$ is the particle radius of cluster m in the matrix phase, $c_{m\beta}$ is the volume concentration of clusters m like $c_{1\beta}$, and $D_{(m)}$ is the diffusivity of mobile clusters m. The capture radius is always approximated as the sum of cluster radius of the two clusters in reaction ($R_n + R_m$) [5, 6].

The emission coefficients $w^{(-)}_{(n+m)-(m),(n)}$ are defined as:

$$w^{(-)}_{(n+m)-(m),(n)} = w^{(+)}_{(n)+(m),(n+m)} exp\ (\frac{\sigma(n+m)-\sigma(n)-\sigma(m)}{k_B T}) \quad (18)$$

Again, here we consider the diffusion-controlled phase transition kinetics,

$$w^{(+)}_{(n)+(m),(n+m)} = 4\pi(R_n + R_m) D_{(m)} c_{m\beta} \quad (19)$$

When we treat $f(n,t)$ as the number of clusters per unit site volume of the matrix phase, then $c_{m\beta}$ becomes $f(m,t)/\Omega$. And the flux $J_{(n)+(m),(n+m)}$ is now:

$$J_{(n)+(m),(n+m)} = 4\pi(R_n + R_m) \frac{D_{(m)}}{\Omega} f(m,t) f(n,t) - 4\pi(R_n + R_m) \frac{D_{(m)}}{\Omega} exp\ (\frac{\sigma(n+m)-\sigma(n)-\sigma(m)}{k_B T}) f(m,t) f(n+m,t) \quad (20)$$

3.3 Parameters for the Cu in Fe Cluster Dynamics model

All the parameters used in the cluster dynamics model for Cu in Fe are given in this section.

The impurity diffusivity of Cu in pure Fe as an important input parameter for cluster dynamics simulations. All the original experimental measurements [7-17] are reviewed and replotted in Figure 1. In the present work, the diffusivity is extrapolated from the high temperature diffusivity data and meanwhile take into consideration of the atomistic kinetic Monte Carlo simulation data [18] at low temperature since the data may have certain rationality. The low temperature data are used to check the general trend of the extrapolation. The diffusivity of Cu in Fe used in the present work is also shown in Figure 1 indicated by the extrapolated solid line, which is given by $D_{Cu} = 2.14 \times 10^{-4} exp\ (\frac{-253000}{8.3145T})$.

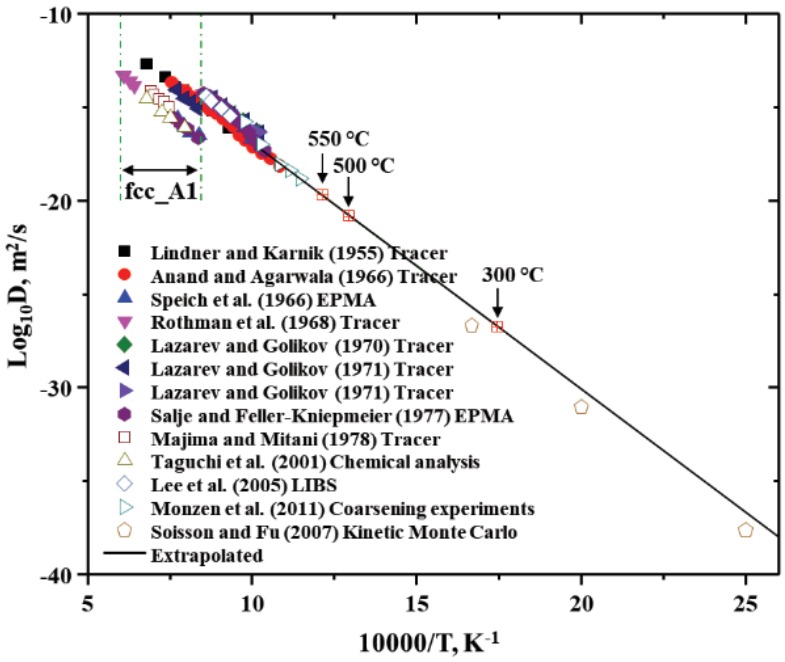

Figure 1. Impurity diffusivity of Cu in Fe.

In the present work, the diffusivities of Cu clusters are taken from the simulation work by Soisson and Fu [18] with modification as will be discussed later. No other data sources are available for these diffusivities, and more work validating these values is likely useful. The diffusivity for small particle size is fitted to the atomistic kinetic Monte Carlo simulation results [18] by an exponential function, and a different functional form is fit to data for large particles.

The diffusivity of clusters is then given as:

$$D_n = min(D_1, D_2) \tag{21}$$

where D_1 and D_2 are given as:

$$D_1 = D_{Cu} n^{exp\,(-0.0049T+3.28)}$$

$$D_2 = 7.14 \times 10^{-5} exp\,(\frac{-2.65}{k_B T}) exp\,(\frac{0.7}{k_B T}) n^{-\frac{4}{3}}$$

Figure 2 shows the calculated cluster mobility of Cu from Eq. (21) compared with the atomistic kinetic Monte Carlo simulation results [18] at different temperatures.

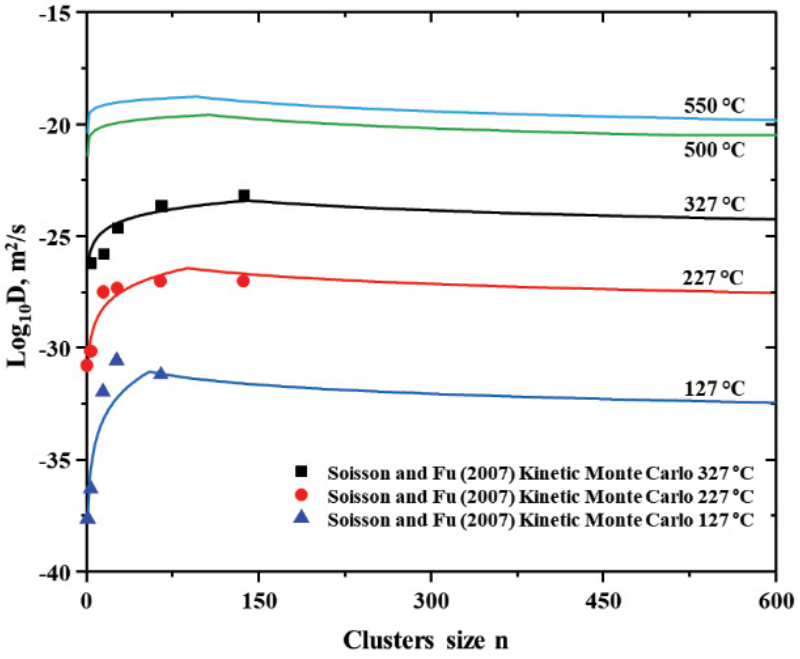

Figure 2. Calculated Cu cluster mobilities from Eq. (21) along with the kinetic Monte Carlo simulation results [18].

The solubility data of bcc_A2 Cu in bcc_A2 Fe solution was taken from the simulation work by Soisson and Fu [18] as $C_{Cu}^{sol}(Fe) = exp(1)\, exp\,(\frac{-0.545}{k_B T})$.

The Cu precipitate interfacial energy and upper limit of clusters that are mobile is taken as parameters to be adjusted. Interfacial energy of 0.5 J/m^2 is set to a reasonable value, consistent with previous studies. Table 1 lists the values used for Fe-1.34 at.% Cu alloy at 500 °C.

Table 1 Model parameters utilized to study the cluster dynamic model.

Temperature (°C)	500
Alloy composition (at.%)	1.34
Interfacial energy of Cu precipitates (J/m^2)	0.50
Diffusivity of Cu monomer (m^2/s)	1.55×10^{-21}
bcc_A2 Cu solubility limit in bcc_A2 Fe (at.%)	0.076 [18]

4. RESULTS

In this section, we present the simulation results for Cu precipitation where we integrate Cu cluster mobility. We explore the effects of interfacial energy, diffusivity, Cu solubility limit in the matrix phase, initial Cu concentration in the matrix phase, and maximum mobile cluster size (n_{max}) on the precipitate evolution, including Cu concentration, mean Cu cluster radius, Cu precipitate number density, and Cu precipitate volume fraction. We use our current cluster dynamics model and consider just isothermal conditions at 500 °C. Since there are a large volume of experimental measurements of the precipitation of Cu in Fe-Cu alloys with a Cu content close to 1.34 at.% at 500 °C in the literature, here we use Fe-1.34 at.% Cu alloys as a model alloy to test the model. To focus on the most uncertain parameters in the model only the test results related to interfacial energy and n_{max} are presented. Note that in this report the analysis of the cluster dynamics simulations excludes clusters of size less than 65 atoms in the calculation of precipitate metrics of size, number density, and volume fraction. This cutoff is chosen to mimic the fact that most experimental methods (e.g,. atom probe, small angle neutron scattering) cannot see very small particles and therefore do not include them in experimental microstructure statistics.

4.1 Interfacial energy effects

Interfacial energy (σ) is very difficult to measure but a critical parameter controlling the precipitation process, and it generally must be fit as any quantitative precipitation modeling effort. The critical nucleus size, nucleation rate, growth rate, and coarsening rate are all interfacial energy dependent [19, 20]. As we are exploring a new model that includes cluster mobility, we studied the effect of interfacial energy on the Cu precipitate evolution within this new model. The results are shown in Figure 3, with interfacial energy in the range of 0.38-0.54 J/m^2. Increasing interfacial energy has strong impact on the volume fraction and concentration profiles of the matrix phase and leads to sharp change in the profiles vs. time during annealing. The number density and mean radius are less significantly affected, but still impacted significantly. In general, lower interfacial energy leads to more rapid nucleation, larger volume fraction at shorter time scales, and smaller radii and large number densities. Our calculation indicates that the general role of interfacial energy is similar to that observed in previous studies for models where only the Cu monomer is mobile.

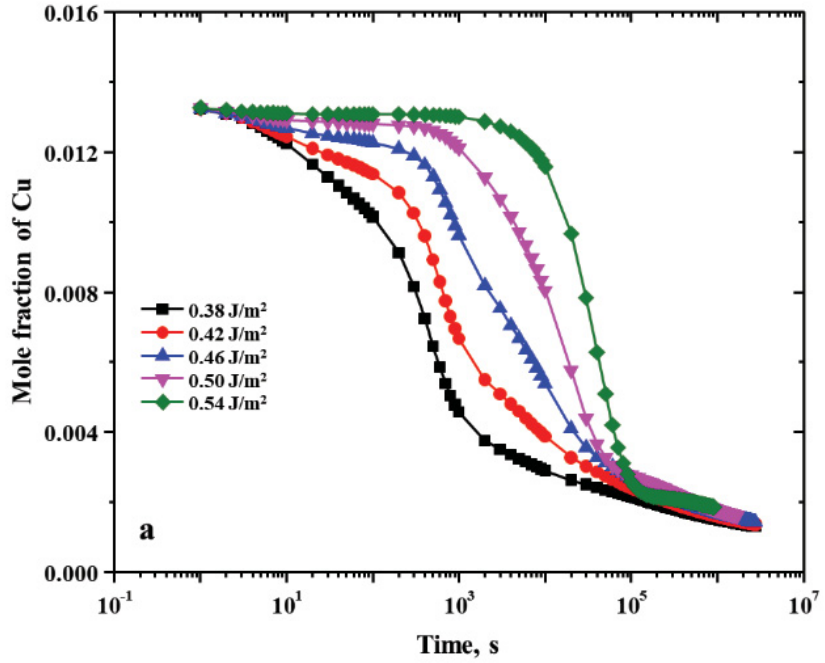
0.016
0.012
0.008
0.004
0.000
Mole fraction of Cu
0.38 J/m²
0.42 J/m²
0.46 J/m²
0.50 J/m²
0.54 J/m²
a
10⁻¹
10¹
10³
10⁵
10⁷
Time, s

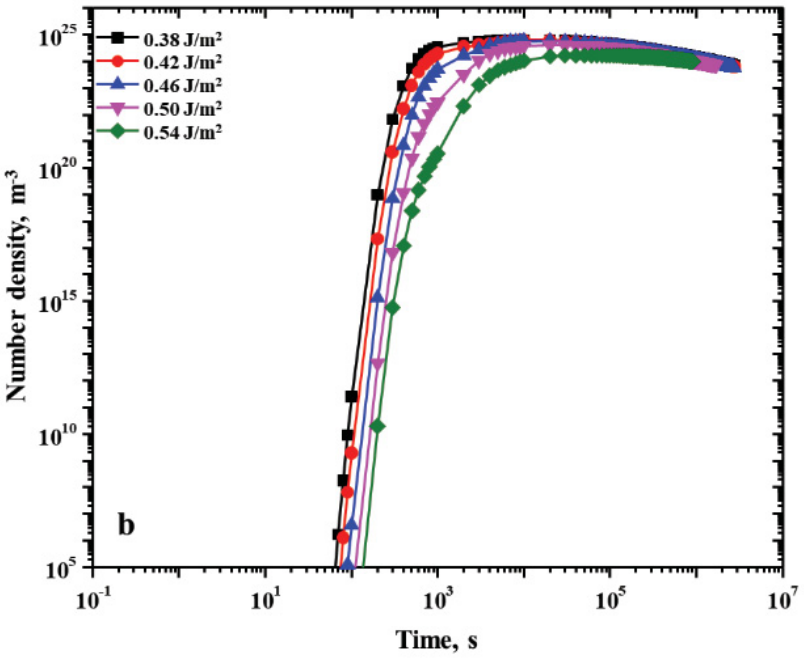
10²⁵
10²⁰
10¹⁵
10¹⁰
10⁵
Number density, m⁻³
0.38 J/m²
0.42 J/m²
0.46 J/m²
0.50 J/m²
0.54 J/m²
b
10⁻¹
10¹
10³
10⁵
10⁷
Time, s

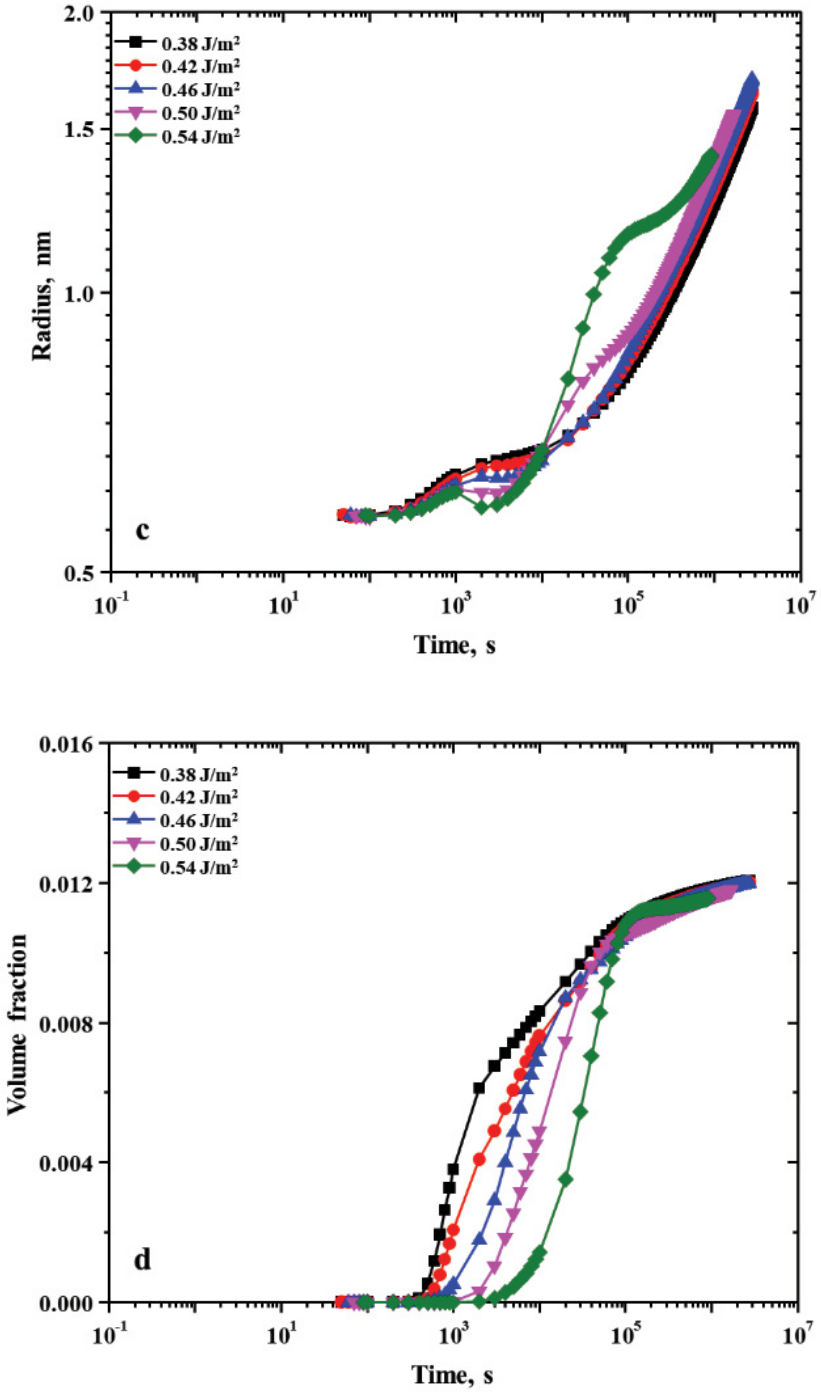

Figure 3. Effect of interfacial energy on time evolution of (a) matrix Cu concentration, (b) mean radius, (c) number density, and (d) volume fraction of Cu precipitates in Fe-1.34 at.% Cu alloy at 500 °C with n_{max}=50.

4.2 **Cluster mobility effects**

In metallic system, it is generally thought that monomers are the only particles that are mobile during precipitation reaction. This is true for some alloy systems like Al-Sc and Al-Zr [21]. However, there is evidence from both theoretical and numerical analysis that monomers are not the only mobile particles in Fe-Cu alloys [4, 18, 22]. However, it is not clear up to what size clusters are mobile, as larger clusters are likely to get impurities at their interface and become immobile through pinning. Here we take the upper limit of clusters that are mobile (n_{max}) as variable to check its influence on the kinetics of Cu precipitation in Fe-1.34 at.% Cu alloy at 500 °C.

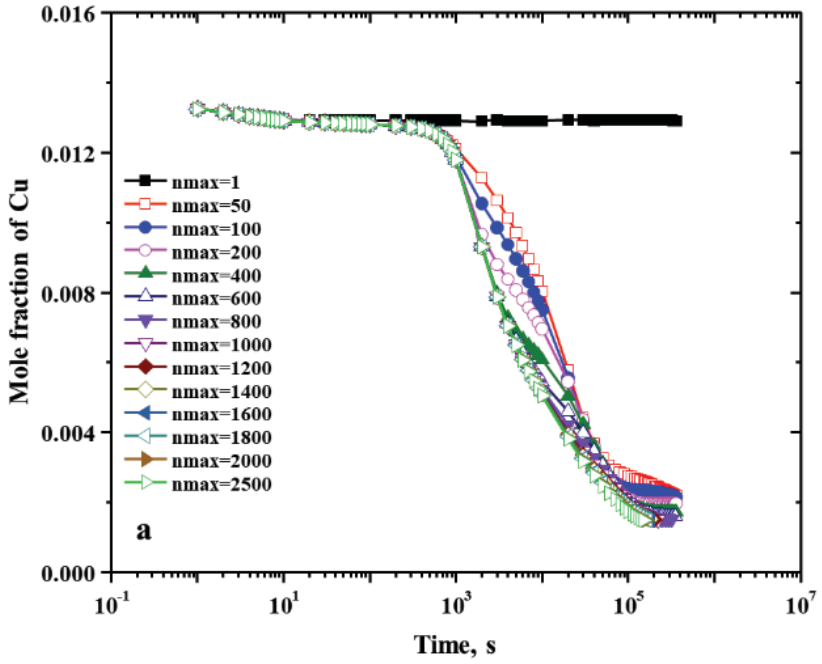

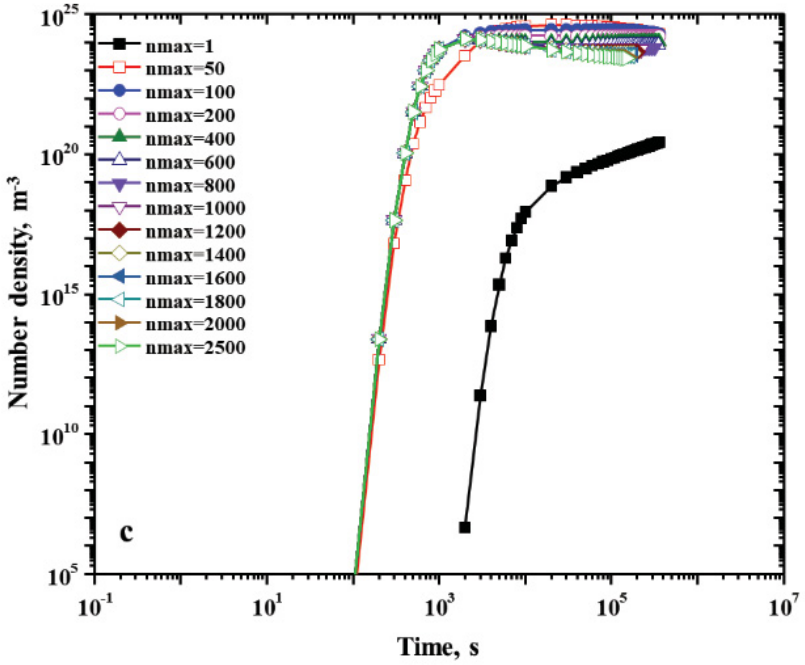
Number density, m-3
Time, s
c
nmax=1
nmax=50
nmax=100
nmax=200
nmax=400
nmax=600
nmax=800
nmax=1000
nmax=1200
nmax=1400
nmax=1600
nmax=1800
nmax=2000
nmax=2500

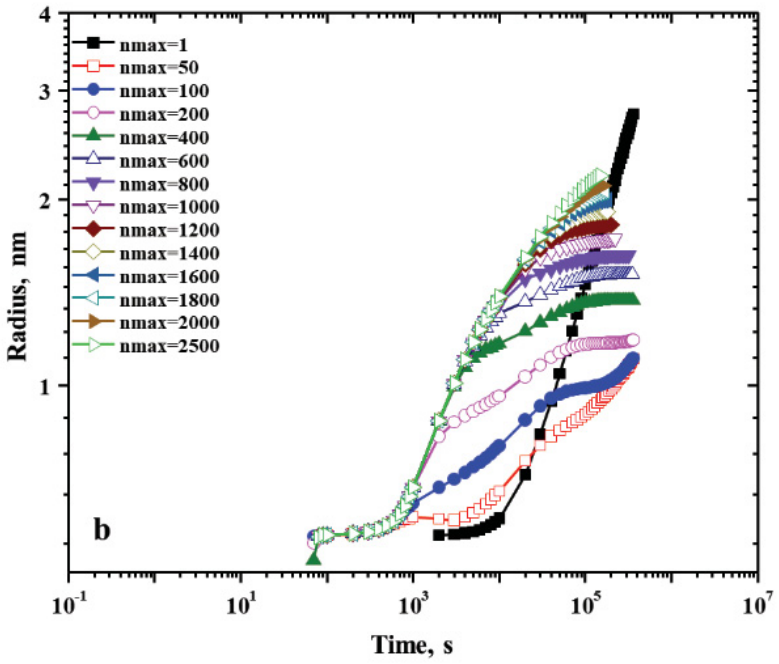
Radius, nm
Time, s
b
nmax=1
nmax=50
nmax=100
nmax=200
nmax=400
nmax=600
nmax=800
nmax=1000
nmax=1200
nmax=1400
nmax=1600
nmax=1800
nmax=2000
nmax=2500

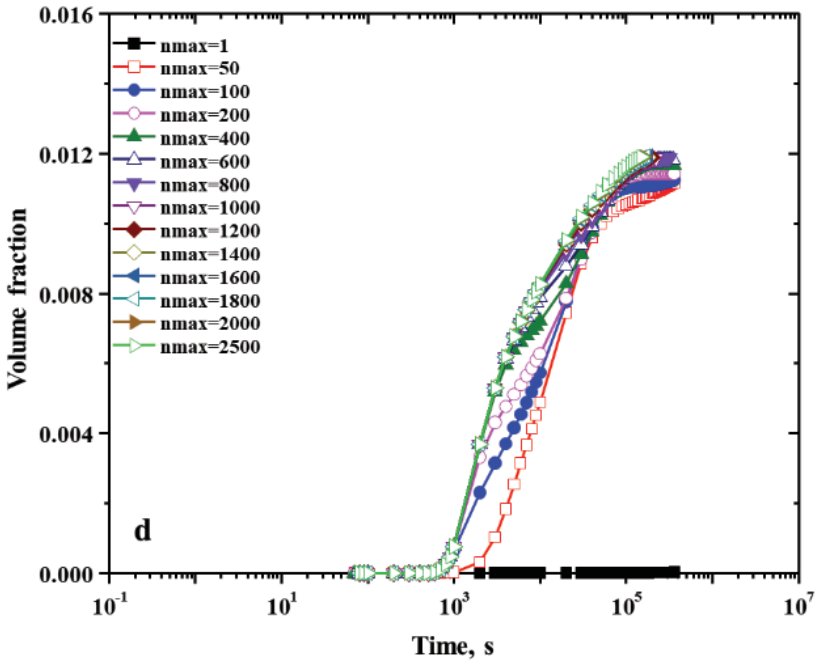

Figure 4. Effect of n_{max} on time evolution of (a) matrix Cu concentration, (b) mean radius, (c) number density, and (d) volume fraction of Cu precipitates in Fe-1.34 at.% Cu alloy at 500 °C with σ=0.5 J/m^2.

Figure 4 shows the calculated results with n_{max} from 1 to 2500, and demonstrates that the precipitation kinetics is substantially enhanced by cluster mobilities. When only considering the mobility of monomer, the mean radius grows steeply following predominantly grows as an $\bar{R} \propto t^{\frac{1}{2}}$ law. However, when using reasonable model parameters, the volume fraction and number density of precipitates are unreasonably low. With the introduction of cluster mobility, the matrix composition, mean radius, number density, and volume fraction evolution profiles are substantially modified. With increasing n_{max} the precipitation initiates at a much early time and the mean radius and volume fraction also show shape changes, with the most dramatic changes occurring by n_{max} =50. When an n_{max}>1 the number density of precipitates shows a peak around 10^{24}/m^3, which is much more consistent with known experiments (see Sec. 4.3) than when n_{max}=1. It is interesting to see that the matrix composition, mean radius, and volume fraction evolution profiles each convergence to a limiting profile as n_{max} increases. This phenomenon also happens for number density for early times before 2×10^3 s, although larger n_{max} continues to have effects for later times.

4.3 Assessment against experiment – modeling precipitation in Fe-1.34 at.% Cu alloy

Fe-Cu alloy with Cu content close to 1.34 at.% is widely used as model alloy to study the precipitation kinetics [23-31] in Cu containing steel. Previous modeling efforts with both cluster dynamics and (Kampmann-Wagner Numerical) KWN methods have shown that to match experiments a large Cu diffusivity sometimes several order of magnitude above that measured by more direct methods is required [22, 29, 32]. In the present work, we fixed the Cu diffusivity and solubility to values that are generally quite well constrained by previous experiments (see Sec. 3.3) and explored how well we could model the precipitation data by changing just the most poorly constrained model parameters, which are interfacial energy, maximum size of mobile clusters, and the cluster mobility of larger clusters. The available experimental information is summarized in Figure 5. It can be seen from the diagram that the experimental number density and volume fraction are generally consistent except for the data from Warczok et al. [31], where a very large number density was reported at very short aging time and the calculated volume fraction is also very large compare to other work [23, 24, 29]. Therefore, while we will include this data in discussion as useful, we do not consider it reliable and do not attempt to fit to it. The measured mean radius from different recourses are in good agreement at long annealing time (above 4×10^3 s). At low annealing time, the mean radius falls into two groups. One group is represented by Kampmann and Wagner [24] and Perez et al. [30]. The other is Warczok et al. [31], Charleux et al. [28] and Osamura et al. [26]. After extensive parameter exploration we found a set of values that yield a good description of the precipitate evolution over the time scale we calculated, which includes up to 10^5 s. The parameters are an interfacial energy of 0.5 J/m^2, n_{max}=9000, D_{Cu}=1.55×10^{-21} m^2/s, and cluster diffusivity described by Eq. (21). In addition, we made modification to the cluster diffusivities from Eq. (21). In general we found that we were not able to match the experimental data well using just Eq. (21). One possible cause is that for larger clusters with many hundreds of atoms, Eq. (21) predicts increasingly small diffusivities, which effectively pin the clusters. While this may be correct, it is also very uncertain, since the kinetic Monte Carlo data used in fitting Eq. (21) does not extend to clusters above 150 atoms. Given this uncertainty in the prediction of slow cluster motion, we chose to set a lower bound for the cluster mobility, which we fit to give 10-20.5 m2/s. In practice, this means we take cluster diffusivities from Eq. (21) until clusters of size 517 atoms, at which size we start using a constant diffusivity of 10-20.5 m2/s. The calculated results are shown in Figure 5, where we can see that the model-predicted results are very well matched with the most

reliable experimental data. We note that the radius deviates from the most robust experiments significantly for times before 103s. However, this region is strongly influenced by the exact cutoff we choose for excluding some clusters in the averaging of radius, which here is set to 65 atoms. For example, a cutoff of excluding less than 10 atoms gives much better agreement at these early times, without reducing the agreement at later times. This suggests that some refinement of this cutoff for these specific data sets would be a useful focus of future work. Overall, these results suggests that by including Cu cluster mobility up to a critical size it is possible to successfully model Cu precipitate evolution without utilizing unphysical Cu diffusivities.

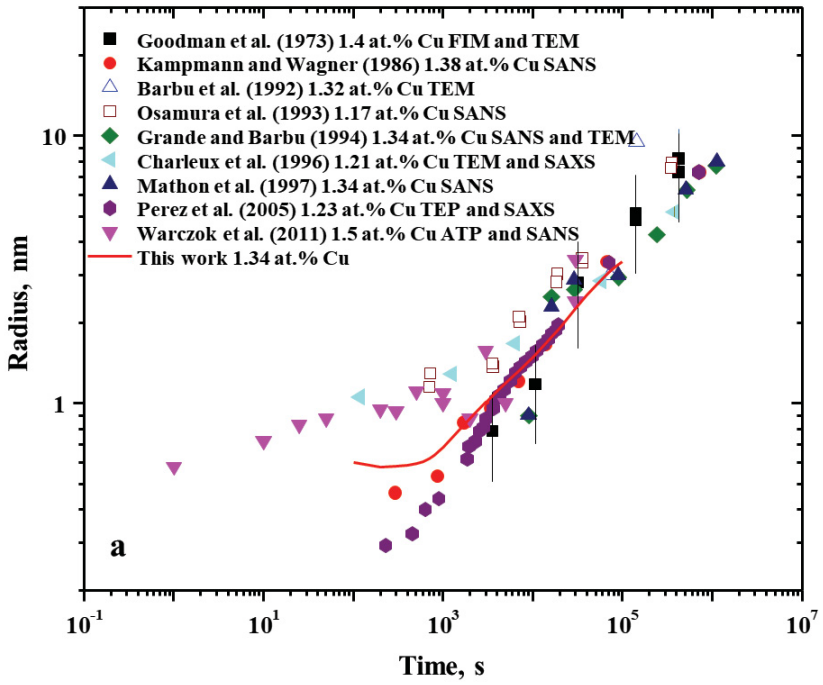

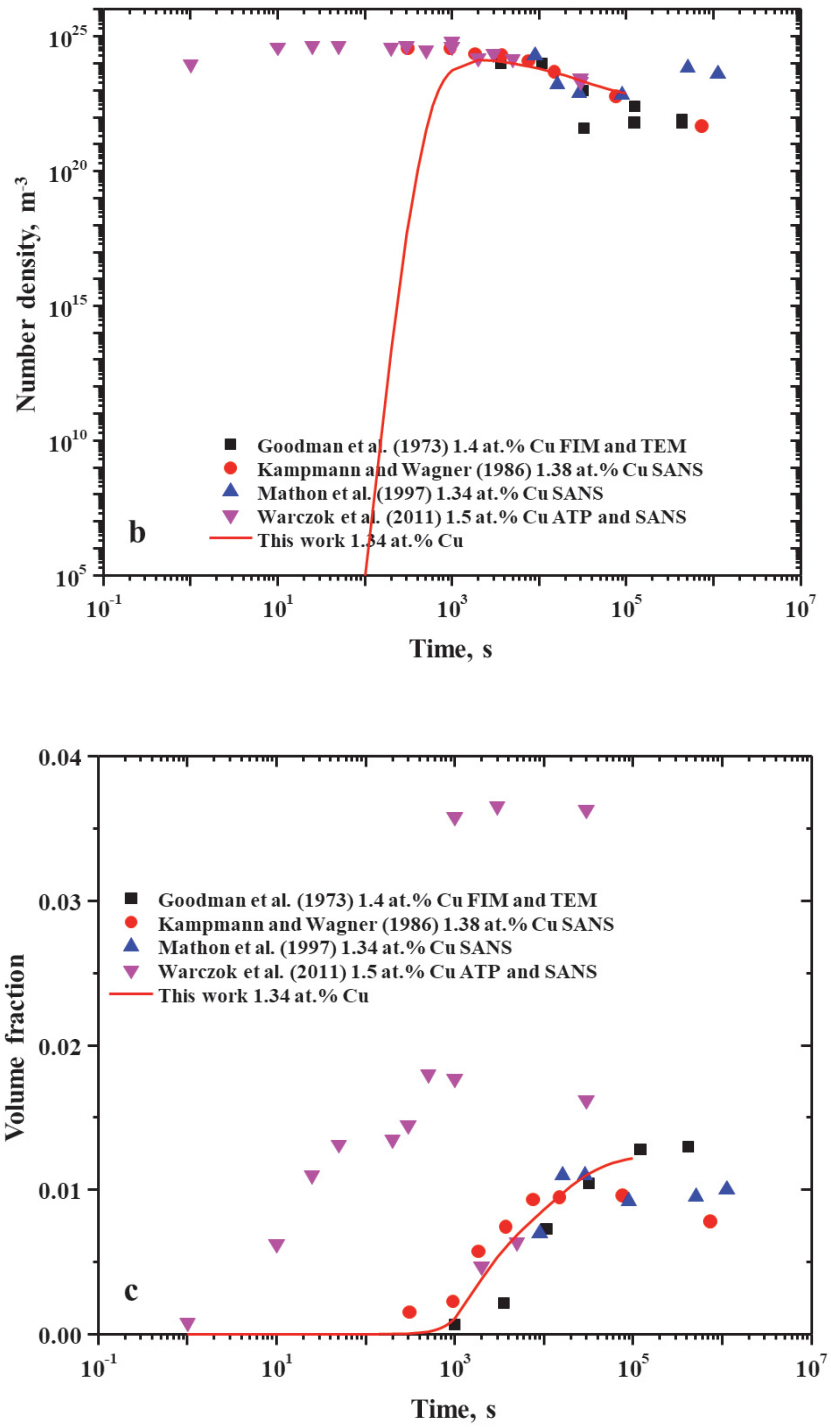

Figure 5: Calculated time evolution of (a) mean radius, (b) number density, and (c) volume fraction of Cu precipitates in Fe-1.34 at.% Cu alloy at 500 °C compared with experimental data.

5. DISCUSSION AND SUMMARY

The current project updated the developed cluster dynamics model for RPVs steel to include mobility of clusters. Important parameters related to the cluster dynamics model were tested to study the effects of each parameter on matrix composition, mean radius, number density, and volume fraction of precipitates. The newly developed model was tested against experimental data for Fe-1.34 at.% Cu alloy under thermal annealing at 500 °C. A set of parameters consistent with previous experimental data was found that can simulate the experimental data with good agreement. These results suggest that the currently developed model is effective for modeling Cu precipitation in steels and can avoid the unreasonably high Cu diffusivity often needed to match experimental Cu precipitate evolution trends.

6. FUTURE WORK

Future work is not planned at present due to lack of funding. However, if funding becomes available, a focus could be in improving the CD model we have been developing (discussed in previous reports), including removing minor approximations we have made, identifying and fixing the source of errors in low-solute and intermediate Ni alloys, very high flux ATR1 condition simulations, and Cu diffusion (as discussed here), enhancing the model beyond simple p-scaling for treating radiation enhanced diffusion, and refining the model by fitting to both all the available microstructural data and to the IVAR hardening database through empirical mechanical property models. This improved model could then be further adapted and refined for modeling thermal annealing behavior to assist in mitigation efforts. We would also like to further refine our machine learning approach (discussed in previous reports), exploring the promise of Gaussian Process Regression. The machine learning models could be tested and improved by using virtual data of hardening vs. flux, fluence, temperature and composition that include both measured conditions, e.g., like those in IVAR, and unmeasured LWR conditions. These virtual data sets could be generated by models like our CD model and can be used to test the predictive ability of the machine learning approaches.

References

[1] M. Mamivand, H.B. Ke, S. Shu, D. Morgan, G.R. Odette , P. Wells, N. Almirall, Incorporation of copper-rich precipitation model into developed Ni-Mn-Si precipitate development models, Light Water Reactor Sustainability Program, September 30, 2016 Milestone 2016.
[2] V.V. Slezov, Kinetics of First-Order Phase Transitions, DOI (2009) 1-38.
[3] V.V. Slezov, J. Schmelzer, Kinetics of formation and growth of a new phase with a definite stoichiometric composition, J. Phys. Chem. Solids, 55 (1994) 243-251.
[4] T. Jourdan, F. Soisson, E. Clouet, A. Barbu, Influence of cluster mobility on Cu precipitation in α-Fe: A cluster dynamics modeling, Acta Materialia, 58 (2010) 3400-3405.
[5] E. Clouet, Modeling of Nucleation Processes, ASM Handbook, 22A: Fundamentals of Modeling for Metals Processing (2009) 203-219.
[6] J. Lepinoux, Contribution of matrix frustration to the free energy of cluster distributions in binary alloys, Philosophical Magazine, 86 (2006) 5053-5082.
[7] R. Lindner, F. Karnik, Diffusion von radioaktiven Kupfer in technischem Stahl, Acta Metallurgica, 3 (1955) 297.
[8] M.S. Anand, R.P. Agarwala, Diffusion of Copper in Iron, Journal of Applied Physics, 37 (1966) 4248-4251.
[9] V.A. Lazarev, V.M. Golikov, Diffusion of copper in iron and iron-boron and iron-molybdenum alloys, Fiz. Metal. Metalloved., 31 (1971) 885-886.
[10] G.R. Speich, J.A. Gula, R.M. Fisher, Diffusivity and solubility limit of copper in α- and γ-iron, 1966, pp. 525-542.
[11] S.J. Rothman, N.L. Peterson, C.M. Walter, L.J. Nowicki, The Diffusion of Copper in Iron, Journal of Applied Physics, 39 (1968) 5041-5044.
[12] V.A. Lazarev, V.M. Golikov, Diffusion of copper in iron and its alloys, Fiz. Metal Metalloved., 29 (1970) 598-602.
[13] V.A. Lazarev, V.M. Golikov, Bulk and grain boundary diffusion of copper in iron and copper-iron alloys studied by using copper-64, Metod Izotop. Indikatorov Nauch. Issled. Prom. Proizvod., DOI (1971) 65-69.
[14] G. Salje, M. Feller-Kniepmeier, The diffusion and solubility of copper in iron, Journal of Applied Physics, 48 (1977) 1833-1839.
[15] K. Majima, H. Mitani, Lattice and Grain Boundary Diffusion of Copper in γ-Iron, Transactions of the Japan Institute of Metals, 19 (1978) 663-668.
[16] O. Taguchi, M. Hagiwara, Y. Yamazaki, Y. Iijima, Impurity diffusion of Al and Cu in γ-Fe, Diffus. Defect Data, Pt. A, 194-199 (2001) 91-96.
[17] C.-G. Lee, J.-H. Lee, B.-S. Lee, Y.-I. Lee, T. Shimozaki, T. Okino, Measurement of the impurity diffusivity of Cu in Fe by laser induced breakdown spectrometry, Diffus. Defect Data, Pt. A, 237-240 (2005) 266-270.
[18] F. Soisson, C.-C. Fu, Cu-precipitation kinetics in α-Fe from atomistic simulations: Vacancy-trapping effects and Cu-cluster mobility, Physical Review B, 76 (2007) 214102.
[19] J.D. Robson, Modelling the overlap of nucleation, growth and coarsening during precipitation, Acta Materialia, 52 (2004) 4669-4676.
[20] R. Kampmann, R. Wagner, Kinetics of precipitation in metastable binary alloys - theory and application to copper-1.9 at. % titanium and nickel-14 at. % aluminum, Pergamon, 1984, pp. 91-103.
[21] E. Clouet, M. Nastar, C. Sigli, Nucleation of Al3Zr and Al3Sc in aluminum alloys: From kinetic Monte Carlo simulations to classical theory, Physical Review B, 69 (2004) 064109.
[22] G. Stechauner, E. Kozeschnik, Thermo-kinetic modeling of Cu precipitation in α-Fe, Acta Materialia, 100 (2015) 135-146.
[23] S.R. Goodman, S.S. Brenner, J.R. Low, An FIM-atom probe study of the precipitation of copper from lron-1.4 at. pct copper. Part I: Field-ion microscopy, Metallurgical Transactions, 4 (1973) 2363-2369.
[24] R. Kampmann, R. Wagner, Phase Transformations in Fe-Cu-Alloys -SANS-Experiments and Theory, Springer Berlin Heidelberg, Berlin, Heidelberg, 1986, pp. 73-77.

[25] T.N. Lê, A. Barbu, D. Liu, F. Maury, Precipitation kinetics of dilute FeCu and FeCuMn alloys subjected to electron irradiation, Scripta Metallurgica et Materialia, 26 (1992) 771-776.
[26] K. Osamura, H. Okuda, M. Takashima, K. Asano, M. Furusaka, Small-Angle Neutron Scattering Study of Phase Decomposition in Fe–Cu Binary Alloy, Materials Transactions, JIM, 34 (1993) 305-311.
[27] N.S.-D. grande, A. Barbu, Study of Cu precipitation mechanisms in Fe-Cu 1.34% at. alloy under electron irradiation, Radiation Effects and Defects in Solids, 132 (1994) 157-167.
[28] M. Charleux, F. Livet, F. Bley, F. Louchet, Y. Bréchet, Thermal ageing of an Fe–Cu alloy: Microstructural evolution and precipitation hardening, Philosophical Magazine A, 73 (1996) 883-897.
[29] M.H. Mathon, A. Barbu, F. Dunstetter, F. Maury, N. Lorenzelli, C.H. de Novion, Experimental study and modelling of copper precipitation under electron irradiation in dilute FeCu binary alloys, Journal of Nuclear Materials, 245 (1997) 224-237.
[30] M. Perez, F. Perrard, V. Massardier, X. Kleber, A. Deschamps, H. de Monestrol, P. Pareige, G. Covarel, Low-temperature solubility of copper in iron: experimental study using thermoelectric power, small angle X-ray scattering and tomographic atom probe, Philosophical Magazine, 85 (2005) 2197-2210.
[31] P. Warczok, D. Reith, M. Schober, H. Leitner, R. Podloucky, E. Kozeschnik, Investigation of Cu precipitation in bcc-Fe – Comparison of numerical analysis with experiment, International Journal of Materials Research, 102 (2011) 709-716.
[32] F. Christien, A. Barbu, Modelling of copper precipitation in iron during thermal aging and irradiation, Journal of Nuclear Materials, 324 (2004) 90-96.